Cross-species cortical alignment identifies different types of neuroanatomical reorganization in higher primates

Nicole Eichert[1,*], Emma C. Robinson[2], Katherine L. Bryant[3], Saad Jbabdi[1], Mark Jenkinson[1], Longchuan Li[4], Kristine Krug[5], Kate E. Watkins[6] & Rogier B. Mars[1,3]

[1] Wellcome Centre for Integrative Neuroimaging, Centre for Functional MRI of the Brain (FMRIB), Nuffield Department of Clinical Neurosciences, John Radcliffe Hospital, University of Oxford, Oxford, OX3 9DU, United Kingdom
[2] Biomedical Engineering Department, King's College London, London, WC2R 2LS, United Kingdom
[3] Donders Institute for Brain, Cognition and Behaviour, Radboud University Nijmegen, 6525 HR Nijmegen, The Netherlands
[4] Marcus Autism Center, Children's Healthcare of Atlanta, Emory University, Atlanta, GA 30329, United States of America
[5] Department of Physiology, Anatomy and Genetics, University of Oxford, Oxford, OX1 3PT, United Kingdom
[6] Wellcome Centre for Integrative Neuroimaging, Department of Experimental Psychology, University of Oxford, Oxford, OX2 6GG, United Kingdom

* Correspondence:
Nicole Eichert
Wellcome Centre for Integrative Neuroimaging
Nuffield Department of Clinical Neurosciences
John Radcliffe Hospital
University of Oxford
Oxford OX3 9DU
United Kingdom
E-mail: nicole.eichert@psy.ox.ac.uk

Abstract

Evolutionary adaptations can affect different aspects of brain architecture, including areal expansion, relocation, or changes in connectivity profiles. Distinguishing between different types of reorganization is critical for our understanding of brain evolution. We propose to address this using a computational neuroanatomy approach. We investigate the extent to which between-species cortical alignment based on myelin can predict changes in connectivity patterns across macaque, chimpanzee and human brains. We show that expansion and relocation of brain areas as predicted by the myelin-based alignment are sufficient to predict reorganization of several white matter tracts and their terminations in temporal, frontal and parietal cortex. A notable exception is the arcuate fasciculus, in which we found extensive tract expansion into new territories that cannot be explained by cortical expansion. The presented approach can flexibly be extended to include other features of cortical organization and other species, which allows us to directly test and quantify evolutionary hypotheses.

Introduction

Comparative neuroscience aims foremost to identify how each species' brain adapted to its owner's ecological niche. But the great challenge of the field is to generalize these insights to define a unifying theory of brain evolution that can account for both shared features across brains and specializations of particular lineages or species [1].

Differences in brain organization can come in many forms [2–4] and dissociating them is challenging (Figure 1). For instance, given an ancestral or reference state, local expansions of the cortical sheet can lead to the relocation of homologous areas between two species (Figure 1B, top). As a case in point, human MT+ complex is located much more ventrally in posterior temporal cortex than its macaque homolog [5]. Cortical relocations also affect the connections of these areas, but this situation is distinct from the scenario in which a tract has invaded new cortical territory (Figure 1B, bottom).

Traditionally, different evolutionary scenarios are difficult to distinguish, as this requires data from multiple modalities and from many cortical areas in the species under study. The need for cartography of a large range of species to infer evolutionary principles is well acknowledged [6]. Inferring principles of evolutionary change in brain organization, however, also requires methods to formally compare brains of multiple species.

We propose a framework that allows one to test among different forms of cortical reorganization by registering brains together into a single shared coordinate system. Such an approach allows us to place the different brains into a common space based on one feature and then compare the results to registration based on another feature. This concept proved feasible in a previous study testing whether the extension of the human arcuate fasciculus (AF) compared with the macaque AF could be accounted for by differential expansion between the two brains [7]. In the present study, we generalize this approach to develop a cross-species registration based on a

multimodal surface matching (MSM) algorithm [8–10] to derive a cortical registration between different species.

We based our registration framework on whole-brain neuroimaging data of macaque, chimpanzee and human brains. Neuroimaging allows one to acquire high-resolution data from the same brains using different modalities within a short time. The digital nature of the data allows easy manipulation, making it ideal for the present purposes [11]. As primary modality we use maps of myelin content within the cortical ribbon derived from T1- and T2-weighted scans [12]. Such 'myelin maps' can be used to identify homologous areas across brains and species, such as primary sensory and motor cortex, which is high in myelin, and association cortex which is low in myelin [13,14]. As the second modality, we use diffusion MRI tractography to reconstruct long range white matter fibers of the cortex to establish its connections [15,16].

Given data from these two modalities, we developed an approach to reveal different types of cortical reorganization. First, we register the cortical surfaces of the different species to one another based on myelin maps. Such cortical alignment allows us to use the distinction of primary and higher order areas in myelin maps as anchor points across all three species. Next, we apply this registration to overlay homologous parts of the cortex and to calculate the underlying distortions of the cortical sheet. This distortion field effectively models areal expansion or contraction underlying cortical relocation of homologous areas. We then apply this registration to the cortical projection maps of white matter tracts to assess how well the myelin-based registration can predict changes in tract projection patterns across species. A good prediction indicates that cortical expansion and relocation of targets zones alone can predict tact projections, a poor prediction indicates that the tract is reaching new cortical territory.

Here, we distinguish different scenarios of cortical evolution for a set of white matter tracts. We focus our analysis in particular on tracts terminating in posterior temporal, inferior parietal, and occipital cortex, which have well described myelin markers and cortical connections [13,14,17,18], but are also thought to have undergone substantial reorganization among different primate species [17,18, Roumazeilles et al., in prep.]. In the case of the human arcuate fasciculus (AF), for example, it has been suggested that the tract's projections extended into new areas in the middle temporal lobe [21]. For other tracts, such as the inferior fronto-occipital fasciculus (IFO), however, the tract terminations have been found similar across primates, when they were assessed in relation to a connectivity-based brain parcellation [22]. For the superior longitudinal fasciculus (SLF3), an evolutionary trajectory has been described for the frontal extensions, suggesting that SLF3 reaches more anterior territory in the human [23,24]. All such proposed adaptations in brain organization, however, need to be assessed in relation to other types of reorganization. By applying a cross-species registration we can infer if only cortical relocation was affecting a tract's connectivity profile or if a tract is reaching into new cortical territory.

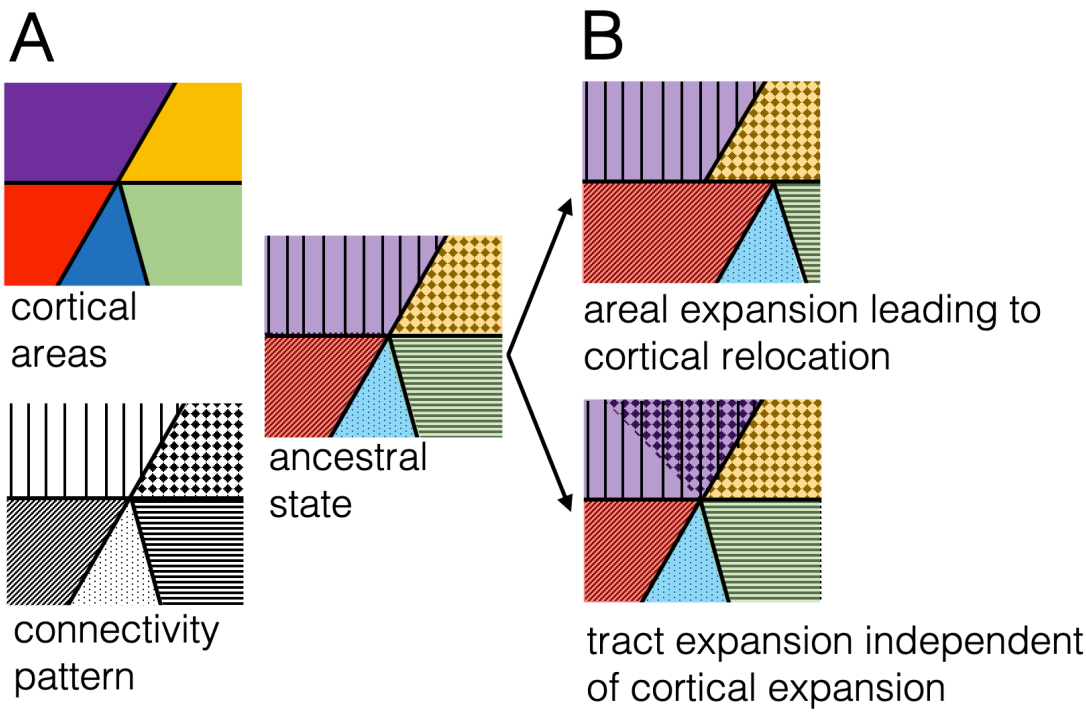

Figure 1. Cortical specializations. **A**: The cortical organization can be described using different modalities such as brain areas defined by myelin content (top) or the pattern of brain connections (bottom). **B**: Anatomical changes can affect both modalities differentially. For instance, at the top the red area has expanded, leading to a relocation of the blue area with respect to the purple and yellow area. The connections do not change in this scenario, resulting in a relocation of the connections of the blue area. In the bottom scenario, the areas have not expanded but the tracts reaching the yellow area have invaded the cortical territory of the purple area. Thus, in both cases the tract termination zones are in different locations than in the ancestral state, but the underlying cause is different.

Results

We set out to investigate different types of cortical reorganization between macaque, chimpanzee, and human brains. First, we investigated cortical expansion of brain areas by registering myelin maps of the cortical surface to one another and investigated the local distortions required. Second, we used the resulting mesh deformations to transform maps of cortical projections of major white matter tracts. This allowed us to assess how well the myelin registration predicts actual projection maps across species, providing an index of tract expansion.

Myelin Registration

We developed a surface registration between species based on myelin maps using MSM. Figure 2 shows the result of the final registration step for chimpanzee-to-human, macaque-to-chimpanzee and macaque-to-human. The cross-species registration aligns the myelin maps well, with the predicted maps showing most of the distinctive features of the actual human myelin map (Figure 2, upper panel). Posterior areas such as V1 are well aligned, with the highest myelin evident on the medial part of the occipital cortex, having relocated quite substantially from a more lateral orientation in the macaque. The prominent myelin hot spot in the location of the MT+ complex is

also noticeable. Areas where the myelin maps showed fewer distinctive features to guide the registration, such as in the prefrontal cortex, showed some differentiation in the projected maps.

The performance of the registration is visualized in the local correlation maps of actual human and predicted myelin maps (Figure 3A). The vast majority of the cortical myelin maps correlates well after applying the registration. The correlation map shows that inferior frontal parts of the cortex and anterior temporal lobe remain most dissimilar. Despite the good alignment of critical posterior landmarks, such as V1 and MT+ complex, the correlation in posterior parietal areas is lower than in more central areas indicating some residual dissimilarity in the registered myelin maps.

The deformations underlying the registration can be visualized using a surface distortion map, which is based on the logarithmic ratio of mesh triangle size before and after applying the transformation (Figure 3B). These expansions are underlying the shifts that lead to relocation of cortical areas. A value greater 1 indicates a relative increase of the underlying mesh triangles and a value below 1 indicates a relative decrease in size. Note that the overall increase in brain size across species is not accounted for in this calculation so that some areas show a distortion value smaller than 1. The macaque-to-chimpanzee distortion map demonstrates that the largest expansion happened in frontal areas. Other areas that show expansion are parietal cortex, posterior temporal and dorsal medial areas. The largest expansion from chimpanzee to human happened in superior temporal and prefrontal cortex, but the distortions are overall smaller and less extended than from macaque to chimpanzee. The macaque-to-human distortion map shows a similar pattern than chimpanzee-to-human, but indicates a stronger distortion in frontal areas.

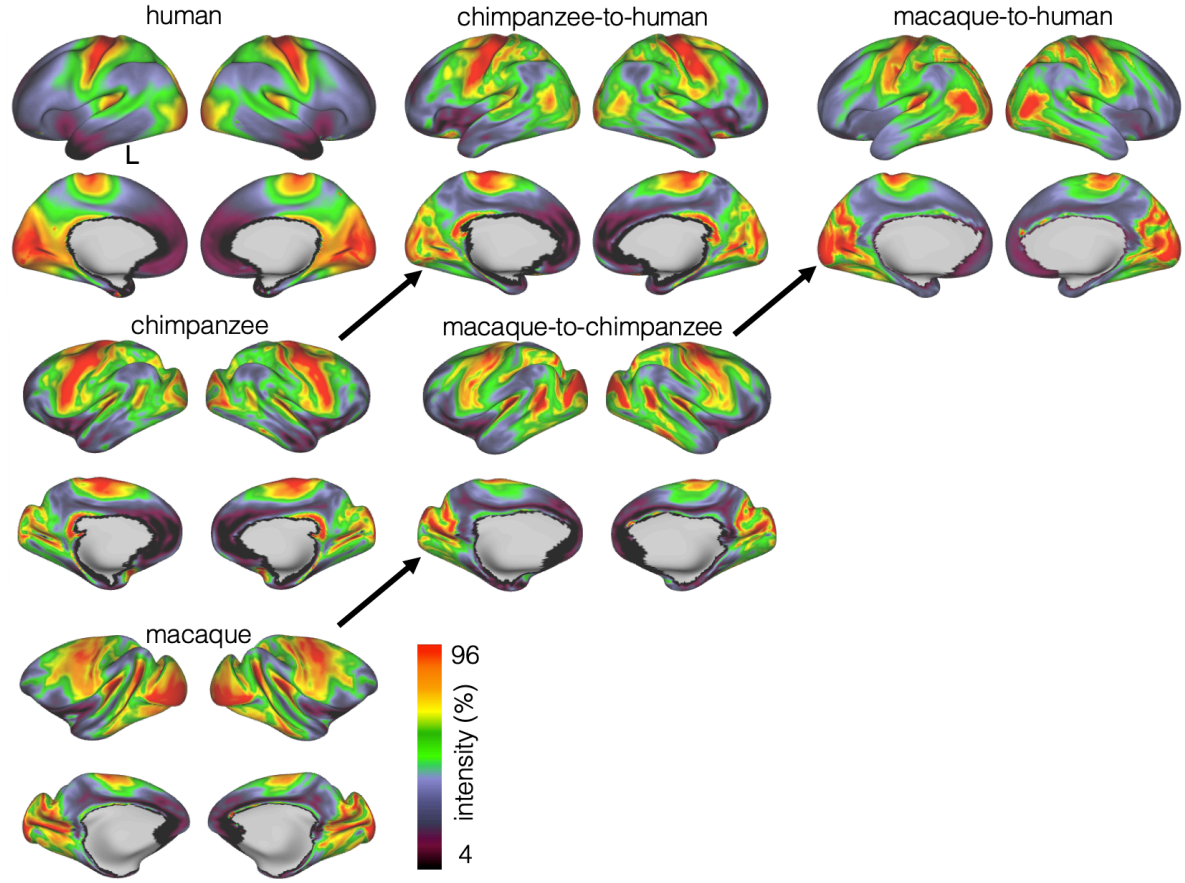

Figure 2. Myelin registration. **A**: Species average myelin maps of the three species (left panel) and myelin maps resampled across species after applying the MSM-derived registration.

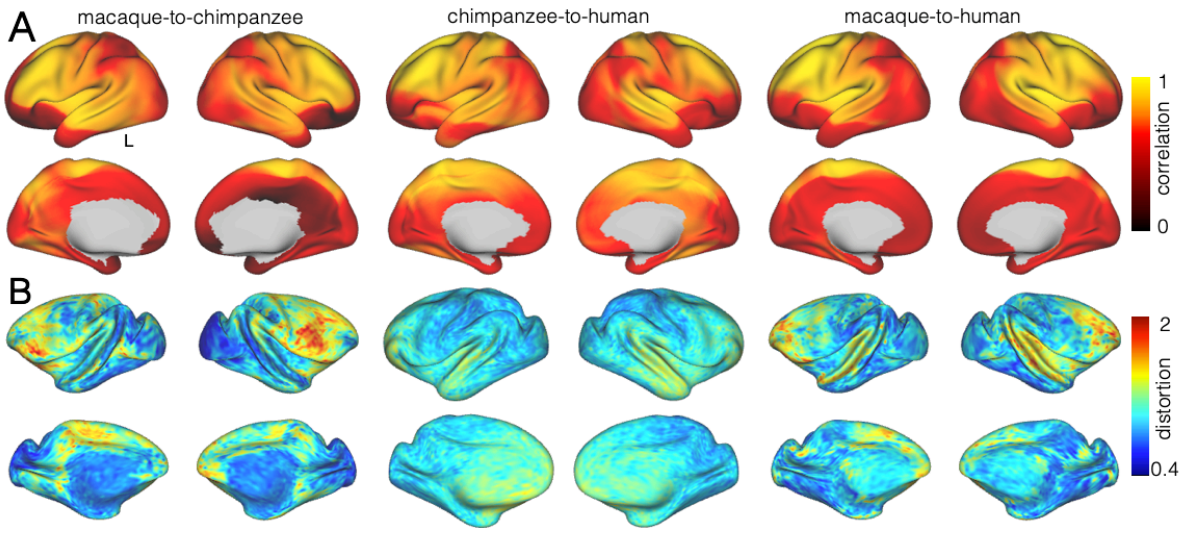

Figure 3. Myelin correlation and mesh distortion. **A**: Local correlation of myelin maps after applying the MSM-derived registration. **B**: Relative distortion of the mesh underlying the registrations. The values indicate a relative expansion (>1) or contraction (<1) of the mesh.

Tract Maps

We constructed the cortical projection maps of the following tracts in all three species: Cortico-spinal tract (CST), middle longitudinal fasciculus (MDLF), vertical occipital fasciculus (VOF) inferior fronto-occipital fasciculus (IFO), inferior longitudinal fasciculus (ILF), the third branch of the superior longitudinal fasciculus (SLF3), and the arcuate fasciculus (AF). We then applied the myelin-based surface registration to assess whether the cortical expansion and relocation demonstrated above fully explains the changes in tracts. Figure 4 shows the actual and predicted tract maps for CST, MDLF and AF in the left hemisphere. Figure 5 shows actual and predicted tract maps for the whole set of tracts. For visual assessment, a thresholded overlay of actual human and predicted tract maps is shown in Figure 6A.

The weighted correlation maps provide a visualization of the quality of the prediction for each tract (Figure 6B, C). A high value means that the myelin registration alone is sufficient to predict a tract's projection in this part of the brain. A low correlation value indicates that reorganization of a tract's connectivity pattern took place in addition to cortical relocation modelled by the myelin registration. We also report a correlation value and the Dice coefficient of similarity (Figure 6D, E) as comparable metrics to characterize how well a tract is predicted across species. Both measures were computed within a thresholded area defined by the actual human tract termination (t = 0.2), but the resulting pattern of values is robust across a range of thresholds (not shown).

For the analyzed tracts, the actual cortical terminations that we derived match the connectivity patterns expected from the literature (Figure 5A, C, E). In general, it can be observed that the myelin-based registration can predict the tract maps well in both hemispheres, with the notable exception of AF. The maps for the macaque are overall less well predicted than for the chimpanzee, as can be seen in the overlay and correlation maps (Figure 6). This effect is also captured in the correlation values and Dice coefficients of similarity, which are generally lower for the macaque (with the exception of SLF3 in the right hemisphere).

In the case of CST, the actual tract projections in the three species show terminations in pre-and post-central gyrus (Figure 4A). For the chimpanzee and macaque, these terminations span a relatively larger portion of the cortex, while in the human the anterior part of the frontal lobe does not show any tract terminations. The macaque CST tract map in the left hemisphere shows a dorsal-ventral split, which is not present in the other species. The frontal difference in the three actual tract maps is related to the relative increase in human prefrontal cortex, which is low in myelin content. After applying the myelin-based registration to the macaque and chimpanzee tract maps of CST, the predicted terminations in human space show strong overlap with the actual human tract map (Figure 5A). The myelin-based registration thus can model the effect of an increased prefrontal cortex on CST tract terminations. This overlap is captured in the weighted correlation maps, which have a high value in areas surrounding the central gyrus (Figure 6B). The correlation value and Dice coefficient for the chimpanzee are relatively high (Figure 6C, D). The dorsal-ventral split in the macaque tract maps is preserved after applying the transformation, which leads to low values in the weighted correlation maps and in the derived metrics. The overall extent of the

tract map around the central sulcus, however, is predicted well for both chimpanzee and macaque.

The myelin-based registration also results in good prediction for tract projections in posterior temporal and parietal areas. The actual human tract terminations of MDLF, for example, span the superior temporal gyrus and reach the inferior parietal cortex (Figure 4B). In the macaque and chimpanzee, the actual MDLF terminations terminate in superior temporal gyrus but reach only into a small part of the inferior parietal cortex. When applying the myelin-based registration, macaque and chimpanzee MDLF are both predicted to reach a comparable portion of the human temporal lobe and parts of both angular and supramarginal gyri of the inferior parietal lobe [25]. The myelin-based registration thus predicts MDLF tract projections well and there is no indication of additional modifications in the tract's connectivity pattern.

A similar observation can be made for the posterior terminations of VOF, IFO, ILF and SLF3. The myelin-based registration can predict the posterior cortical projections of those tracts to a large degree and the predicted cortical terminations of the tracts show a strong overlap with the actual human tract terminations. The termination zones of VOF are found in occipital lobe in all three species. Primary visual cortex has moved from the lateral surface in the macaque to the medial surface in the human, which is modelled well in our myelin registration. When applying the registration, macaque and chimpanzee VOF is predicted to reach posterior and medial parts of the occipital lobe, overlapping well with the actual human tract map. Correlation values and Dice coefficients for VOF are high in both species.

IFO is predicted to reach to anterior frontal and occipital areas. Due to the lower registration performance of the myelin maps in these areas (see above), the anterior frontal terminations have to be interpreted with caution. In line with the overlay maps and the weighted correlation maps, the correlation values and Dice coefficients are relatively high for MDLF, VOF, IFO, ILF and SLF3. Taken together, this suggests that expansion and relocation of brain areas is sufficient to model the posterior cortical terminations of these tracts, while reorganization of the tracts' connectivity patterns plays a minor role in explaining the species differences.

The clearest case of a species difference in a tract was presented by AF (Figure 4C). Human AF reaches anteriorly to inferior and dorsal frontal areas. The posterior projections of human AF reach into middle and inferior temporal cortex. AF in the chimpanzee shows similar frontal terminations, reaching to inferior frontal and, to some extent, to dorsal frontal areas. The posterior terminations are in superior temporal cortex. In the macaque, the frontal terminations are notably reduced and the temporal projections reach superior temporal areas.

For AF, the myelin-based registration does not provide a good prediction of the tract map across species. The predicted tract maps in human space show notable species differences, especially for the macaque. Human AF reaches more anteriorly to inferior and dorsal frontal areas and further inferiorly and anteriorly into the temporal lobe. The correlation map for the chimpanzee shows a good prediction in frontal and parietal areas, but low correlation along the remaining temporal lobe. The tract map for human and chimpanzee demonstrate hemispheric differences in the frontal lobe. The prediction for the right hemisphere tract map in the chimpanzee is notably reduced,

which is unexpected. For the macaque, correlation values in both frontal and temporal lobe are extremely low. AF has the lowest correlation value and Dice coefficient, especially in the macaque, which is in line with overlay and correlation maps. This indicates that expansion and relocation of cortical areas is not sufficient to explain the tract projections of AF, but that the tract invaded new cortical territory in the frontal and temporal lobe.

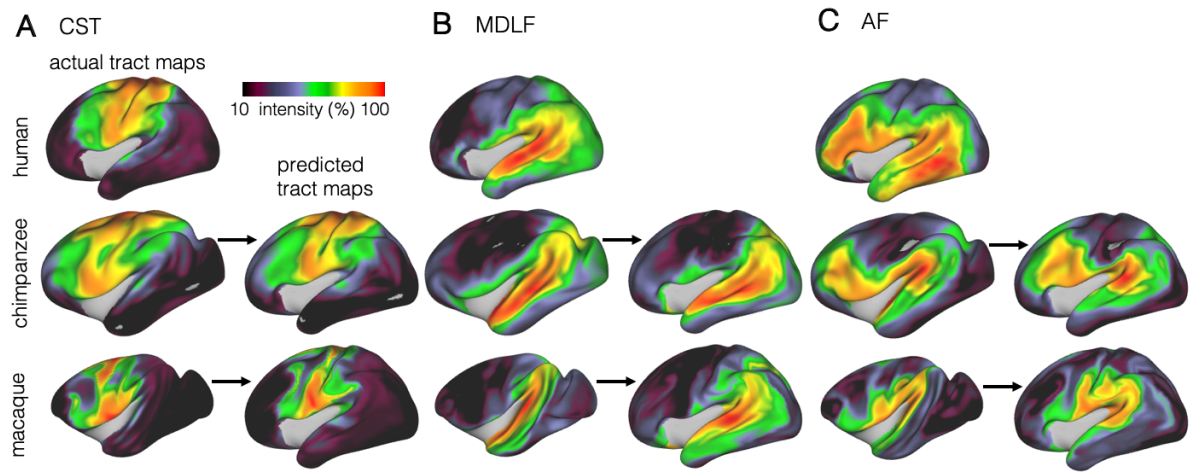

Figure 4. Actual and predicted tract maps. **A**: CST. Left panel: Actual tract maps in human, chimpanzee and macaque. Right panel: Tract maps in human space, predicted by the myelin-based registration for chimpanzee and macaque. **B**, **C**: Results for MDLF and AF using the same layout as in **A**.

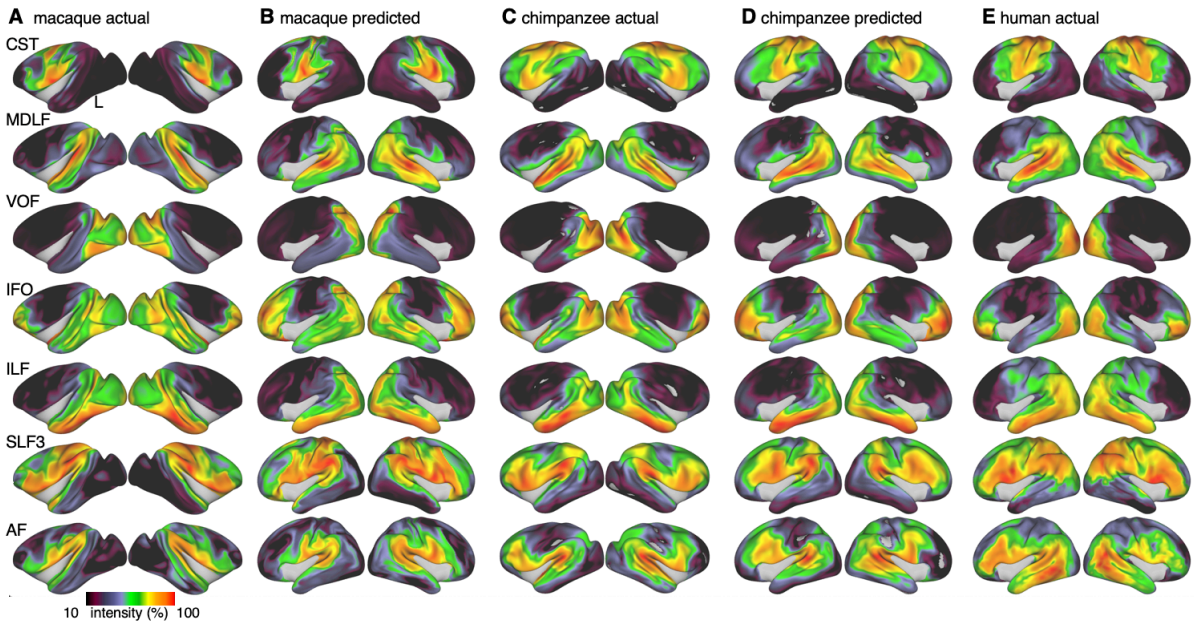

Figure 5. Actual and predicted tract maps. Actual tract maps of macaque (**A**), chimpanzee (**C**) and human (**E**). **B** and **D** show the tract maps in human space, predicted by the myelin-based registration for macaque and chimpanzee.

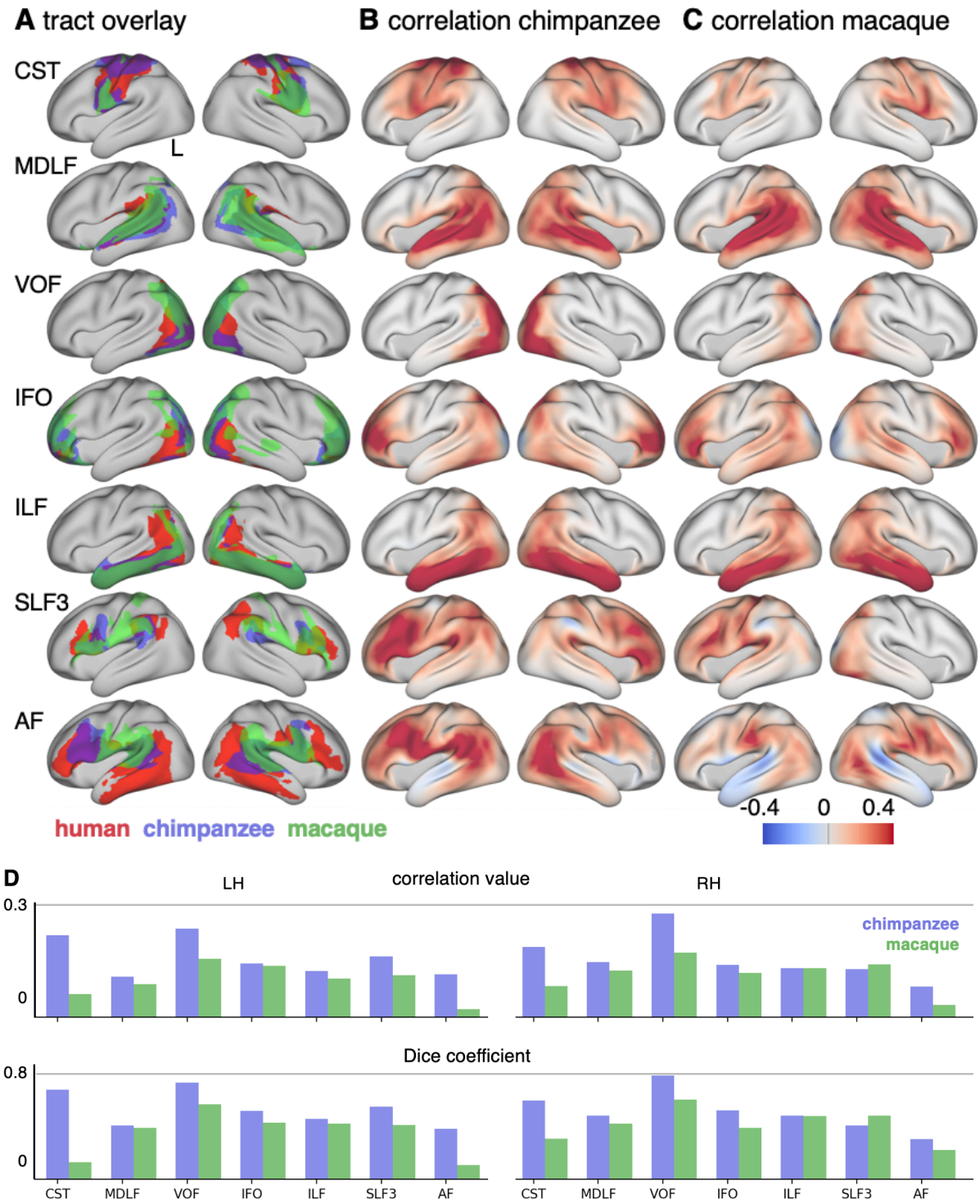

Figure 6. Cross-species comparison results. **A**: Thresholded actual human tract maps (red) and tract maps predicted by the myelin-based registration for chimpanzee (blue) and macaque (green) (thresholds: CST: t = 0.6, MDLF: t = 0.7, VOF: t = 0.6, IFO: t = 0.75, ILF: t = 0.7, SLF3: t = 0.85, AF: t = 0.75). **B**, **C**: Weighted correlation maps of actual human map and predicted chimpanzee and macaque map. **D**: Correlation value (top) and Dice coefficient (below) in the area defined by the actual human tract map thresholded at t = 0.2.

Discussion

The goal of this study was to assess the differential effect of two forms of cortical reorganization to compare brain specializations across species. For this reason, we developed a cross-species surface registration method based on cortical myelin content, which gives us an index of how cortical areas have expanded leading to relocation of cortical areas during evolution. In a subsequent step, we tested if cortical expansion can predict the connectivity patterns of a set of tracts across species. This allowed us to distinguish the effects of cortical expansion from tract expansion (see Figure 1). We showed that expansion and resulting relocation of brain areas alone provide a good prediction of several tracts' terminations in posterior temporal and parietal cortex. In the case of AF in particular, we showed that tract expansion was another driving factor of brain reorganization, in addition to cortical expansion and relocation.

We applied the myelin-based registration to the tract maps in macaque and chimpanzee to transform them into human space. In the case of CST, for example, the human tract projections can be predicted well by our cortical relocation model. This indicates that the pattern of cortical terminations changed according to the general expansion and relocation of brain areas, without additional expansion into new regions of the brain. For tracts reaching to the temporo-parietal areas, such as MDLF, VOF, IFO, ILF, and SLF3, the posterior tract projections can also be modelled well, despite the large distortions of target areas within the cortical sheet. Note that it has previously been shown that SLF3 reaches more anterior territory in the human brain than that of the chimpanzee [23](Bryant, Li & Mars, in prep.), but this seems not to be predicted by our cortical distortion map. However, the result in the frontal cortex is driven by fewer distinct myelin features than those in temporo-parietal cortex and should thus be treated with caution.

AF showed the lowest consistency across species when applying the myelin-based registration. This points to further evolutionary adaptations that specifically affected the connectivity pattern of AF independent of cortical relocation, the scenario described in Figure 1B (bottom panel). Invading new cortical territories changes the unique connectivity fingerprint of an area, which profoundly changes the computational capabilities that area supports [26]. This result is consistent with previous accounts in the literature [7,21] but the approach described here enabled us to formally test this hypothesis in the wider context of cortical reorganization across three primate species and to quantify the species differences. The expansion of AF into middle and inferior temporal cortical territory in the human brain is a hallmark of a number of models of human language processing [27,28], but more recently the role of ventral pathways is also highlighted [29–31]. Here, we show that although both tracts have undergone relocation, the AF in particular invades new cortical territory and thus contributes to new, distinct connectivity fingerprints in the human brain.

The tracts to test in our framework were chosen to have a good spread around the cortex, but our main focus was on temporo-parietal cortex. In fact, our myelin registration provides the best prediction of tract surface projections in the temporal, parietal and occipital cortex. Our approach allows us to explicitly transform data of multiple species into a common space, which makes evolutionary hypotheses directly testable, rather than 'eyeballing' the shared and distinct features. For instance, it has

been previously suggested that the cortical projections of IFO are similar across primates [22], but our results provide more direct evidence for this hypothesis.

With the presented surface matching method, we showed that a registration based on cortical myelin can match critical landmarks across species, despite the substantial deformations involved. The distortion map underlying the registration shows which brain areas expanded most distinctly between species. These expansions are underlying relocation of brain areas. It appears that temporal and frontal areas have relocated most strongly between chimpanzee and human and even more distinctly between macaque and human.

The present approach can successfully model strong cortical expansion and resulting shifts using a region-of-interest-(ROI)-based initialization. We selected ROIs where the literature strongly suggests cross-species homology across primates [13]. Three ROIs were sufficient to bring the myelin maps into rough agreement in preparation for a second alignment step driven by myelin data. We derived a distortion map that models areal expansion leading to cortical relocation. The resulting map is in line with a previously published map of cortical expansion, derived based on the gyral and sulcal pattern in humans and macaques [20]. This is consistent with suggestions that the frontal lobe, temporal lobe and association cortex in general, have expanded disproportionally in the human lineage [3].

We adopted the MSM framework, which is ideally suited to work with multimodal descriptors of the cerebral cortex. It has become a vital tool for human surface registration [32–34] and here we demonstrated its utility for cross-species research. A major benefit of the presented approach is that it can be flexibly modified to include a variety of cortical features, which can be compared across species. Myelin does not provide high contrast in the large human frontal cortex and, as such, it is difficult to provide a good registration in frontal areas. However, the current method can be generalized to any modality of cortical organization, so future studies can incorporate modalities that have greater contrast in this part of the brain such as neurite orientation dispersion and density imaging (NODDI) measures [35] and even resting state fMRI networks [36].

In sum, here we present a framework for analyzing cortical reorganization between brains of different species, applying it in the first instance to cortical relocation of areas due to local expansion and white matter tract connectivity. This allowed us to formalize the changes that occurred in some of the major white matter tracts across different branches of the primate phylogenetic tree, illustrated by data from the Old-World macaque monkey, the chimpanzee great ape, and the human. Future work will expand this approach not only to different modalities, but also to a much wider range of species, which is now becoming increasing possible due to the availability of multi-species datasets [37,38]. This provides a crucial step towards the understanding of phylogenetic diversity across the primate brain.

Materials and Methods

Human data and pre-processing

Human data were acquired in 20 subjects (12 females, 18-40 years) on a 3T Siemens Prisma scanner with a 32-channel head coil. The study was approved by the Central University (of Oxford) Research Ethics Committee (CUREC, R55787/RE001) in accordance with the regulatory standards of the Code of Ethics of the World Medical Association (Declaration of Helsinki). All participants gave informed consent to their participation and were monetarily compensated for their participation.

High-resolution structural images were acquired using a (MPRAGE) T1w sequence (TR = 1900 ms; TE = 3.97 ms; flip angle = 8°; 192 mm FoV; voxel size 1 mm isotropic) and (SPC) T2w sequence (TR = 3200 ms; TE = 451 ms; 256 mm FoV; voxel size 1 mm isotropic; Grappa factor = 2). Diffusion-weighted (DW) MRI data were acquired in a subset of 5 subjects using a sequence from the UK Biobank Project [39]. In brief, we used a monopolar Stejskal-Tanner diffusion encoding scheme [40]. Sampling in *q*-space included 2 shells at b = 1000 and 2000 s/mm^2 (voxel size 2 mm, MB = 3). For each shell, 50 distinct diffusion-encoding directions were acquired (covering 100 distinct directions over the two *b*-values). Five b = 0 images were obtained together with additional three b = 0 images with the phase-encoding direction reversed.

T1w and T2w scans were pre-processed using the HCP-pipeline [41] cloned from the 'OxfordStructural' - fork (https://github.com/lennartverhagen/Pipelines). The processing pipeline includes anatomical surface reconstruction using FreeSurfer and provides measures of sulcal depth and surface maps of cortical myelin content [42,43]. The mean image of the T1w scans was divided by the mean image of the T2w scans to create a T1w/T2w image. The bias corrected T1w/T2w-ratio was mapped onto the mid-thickness surface using Connectome Workbench command-line tools. We refer to this surface map as T1w/T2w 'myelin map' [12,13]. In order to create a human average myelin map, the subject's individual myelin maps were aligned using MSM. The myelin alignment was initialized using alignment based on maps of sulcal depth (parameters are provided in Table S1). To create the species average maps, we used an implementation of MSM that optimizes based on a first-order (pairwise) cost function to penalize against distortions, given that no excessive distortions were expected.

Human volume data were registered to the Montreal Neurological Institute standard space (MNI152) and surface data was transformed to a surface template space (fs_LR).

Chimpanzee Data and Pre-processing

In vivo chimpanzee structural MRI and DW-MRI data were obtained from the National Chimpanzee Brain Resource (www.chimpanzeebrain.org). Data were acquired at the Yerkes National Primate Research Center (YNPRC) at Emory University through separate studies covered by animal research protocols approved by YNPRC and the Emory University Institutional Animal Care and Use Committee (approval no. YER-2001206). These chimpanzee MRI scans were obtained from a data archive of scans obtained prior to the 2015 implementation of U.S. Fish and Wildlife Service and National Institutes of Health regulations governing research with chimpanzees. All the scans reported in this publication were completed by the end of 2012.

T1w/T2w myelin maps were obtained from a group of 29 adult chimpanzees (all female), scanned at 0.8 mm isotropic resolution [13,44]. DW-MRI data were obtained in a subset of five individuals. Acquisition and pre-processing was previously described [45,46]. Two diffusion-weighted images (TR = 5900 ms; TE = 86 ms; 41 slices; 1.8 mm isotropic resolution) were acquired using a single-shot spin-echo echo planar sequence for each of 60 diffusion directions (b = 1000 s/mm^2), each with one of the possible left–right phase-encoding directions and 4 repeats, allowing for correction of susceptibility-related distortion. For each repeat of diffusion-weighted images, five images without diffusion weighting (b = 0 s/mm^2) were also acquired with matching imaging parameters.

Chimpanzee volume and surface data were registered to a standard space template based on 29 chimpanzee scans acquired at the YNPRC [44]. A species average myelin map was derived using MSM as described for the human.

Macaque Data and Pre-processing

Ex vivo DW-MRI data were obtained from four rhesus macaques (one female, age at death: range 4-14 years) using a 7T magnet. Data acquisition and DW-MRI pre-processing have been previously described in detail [7]. Data were acquired using a 2D diffusion-weighted spin echo multi slice protocol with single line readout (DW-SEMS; TE = 25 ms; TR = 10 s; matrix size: 128 x 128; resolution 0.6 mm; number of slices: 128; slice thickness: 0.6 mm). Nine non-diffusion-weighted (b = 0 s/mm^2) and 131 diffusion-weighted (b = 4000 s/mm^2) volumes were acquired with diffusion encoding directions evenly distributed over the whole sphere, except in one monkey were 7 non-diffusion-weighted images and 128 diffusion directions were collected.

Additionally, *ex vivo* data from one male macaque were obtained [47] and pre-processed as described previously [48]. Relevant imaging parameters for DW-MRI data were: 4.7T Oxford magnet equipped with BGA 12 gradients; 3D segmented spin-echo EPI 430 µm isotropic resolution, 8 shots, TE = 33 ms, TR = 350 ms, 120 isotropically distributed diffusion directions, b = 8000 s/mm^2.

To obtain macaque T1w/T2w myelin maps, *in vivo* T1w and T2w scans data were obtained from a previous study on five separate rhesus macaques (4 females, age range 3.4 years - 11.75 years). Data acquisition and pre-processing of the macaque data have been described previously [14]. Procedures of the *in vivo* macaque data acquisition were carried out in accordance with Home Office (UK) Regulations and European Union guidelines (EU directive 86/609/EEC; EU Directive 2010/63/EU).

Macaque surface reconstruction and average myelin maps were derived as described for the human. Macaque volume and surface data were registered to a standard space, which is based on data from 19 macaques acquired at YNPRC [44,49].

Myelin-based Surface Registration

Our aim was to derive a cross-species registration to model expansion and relocation of cortical brain areas. Therefore, we performed registration based on average surface

myelin maps in the three species using MSM with higher-order smoothness constraints [10,50]. We derived a transformation of the cortical surface so that homologous myelin landmarks across species matched. The general processing steps were as follows, but a more detailed description of the methodology is provided in the Supplementary Material.

We obtained a 'chimpanzee-to-human' (illustrated in Figure 7A) and a 'macaque-to-chimp' registration. A 'macaque-to-human' registration was derived as a concatenation of both registration stages to minimize the between-species distortions needed. As input for the registration we used the three species average myelin maps and we performed the registration for both hemispheres separately. We derived these registrations (macaque-to-chimpanzee and chimpanzee-to-human) because they allowed us to directly compare those brains that have the smallest phylogenetic distance. We are, of course, not implying that the three species evolved from one another.

In general, the registration was derived using two stages. The first stage was based on three regions-of-interest (ROIs) to handle the gross distortions that are involved in matching myelin landmarks across species (Figure 7A(2)). Two ROIs captured the highly myelinated precentral motor cortex (MC) and MT+ complex and a third ROI covered the medial wall (MW). We used MSM to obtain a registration so that the ROIs are roughly matched across species (Figure 7A(3)). In the second stage, the ROI-based registration was used as initialization for the subsequent alignment of the whole-hemisphere myelin maps (Figure 7A(4)). To derive a macaque-to-human registration, we resampled the average macaque myelin map to chimpanzee space using the MSM-derived macaque-to-chimpanzee registration. Then we aligned the resampled macaque map in chimpanzee space with that of the human while using the chimpanzee-to-human registration as initialization.

The quality of the registration performance was visualized by computing a local spatial correlation between the human myelin map and the result of the chimpanzee and macaque registration. The correlation was computed using a sliding window around every vertex on the sphere using MATLAB's corrcoef-function (Mathworks, Natick, MA). We used a search kernel of 40° that corresponds to a circular search window with a radius of approximately 7 cm.

To visualize the distortions underlying the three cross-species registrations, we derived a map of surface distortions (Figure 7A(5)). We computed the areal distortion between original and distorted mesh, as implemented in 'wb_command -surface-distortion'. Here, distortions for each mesh face are estimated as $\log_2(A_1/A_0)$, where A_0 is the area of the original mesh face and A_1 is the area of a deformed mesh face. The values per vertex are calculated as a weighted average, where weights are calculated from the relative size of the vertices adjoining mesh faces. We are representing distortions between original and distorted sphere thus the numerical values of the distortion map are not meaningful.

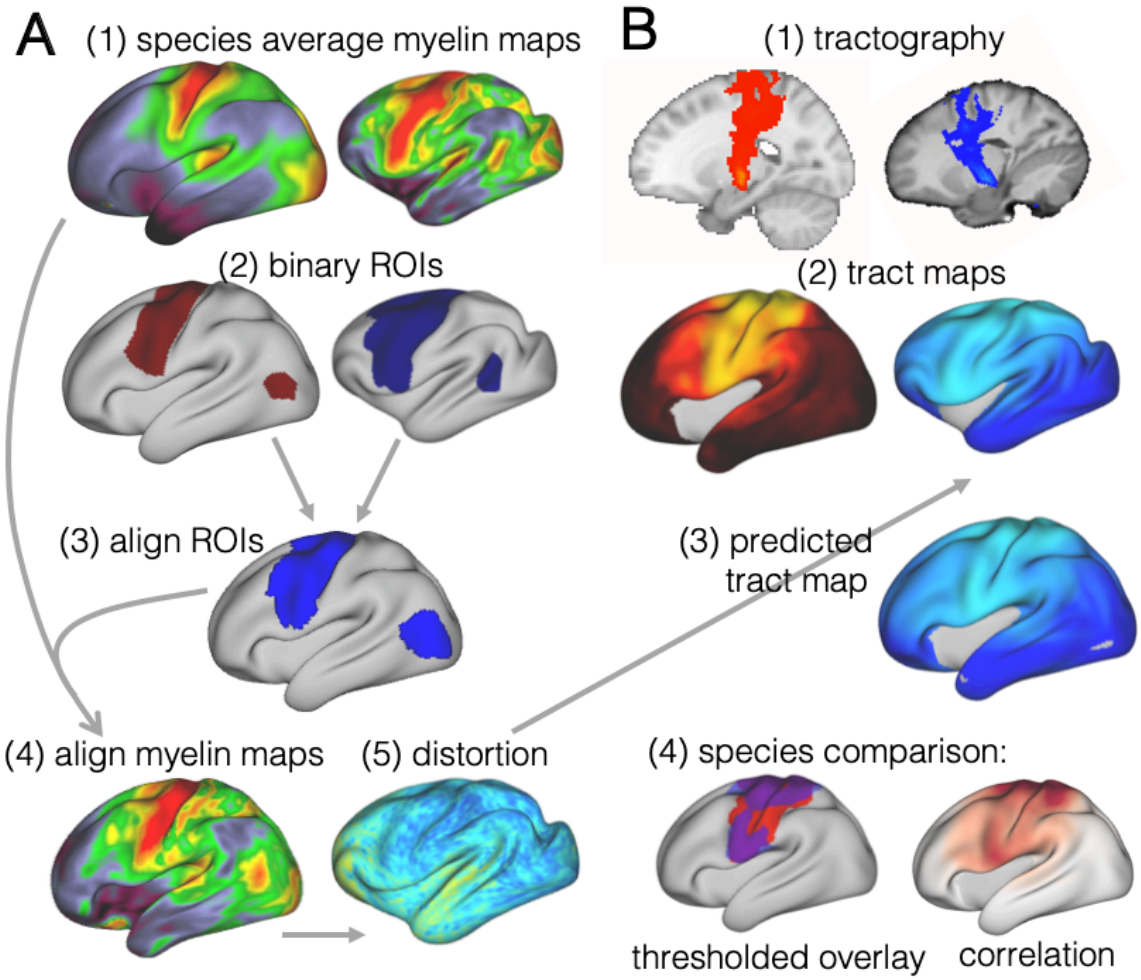

Figure 7. Methods overview. **A**: Myelin-based surface registration for chimpanzee-to-human using MSM. Average myelin maps from human (left) and chimpanzee (right) are aligned in two stages: ROI-based alignment (2-3) followed by alignment of the myelin maps (4). The arrows indicate that both the species average myelin maps and the ROI-based registration are inputs for the alignment of the myelin maps. A distortion map (5) visualizes the deformations underlying the registration. **B**: Tract surface analysis for an example tract (CST). The myelin-based cross-species registration is applied to transform the actual chimpanzee tract map (2) to human space (3). Having both tract maps in the same space allows a direct species comparison (4). The arrow from **A** to **B** indicates the step where the actual chimpanzee CST tract map is transformed to human space by applying the myelin-based registration.

Tractography

Human and chimpanzee DW-MRI data were pre-processed using tools from FDT (FMRIB's Diffusion Toolbox, part of FSL 5.0 [51]). We applied the TOPUP distortion correction tool followed by eddy-current distortion and motion correction [52,53] as implemented in FSL. Macaque *ex vivo* DW-MRI data were processed using tools from FSL as implemented in an in-house MR Comparative Anatomy Toolbox (Mr Cat, www.neuroecologylab.org).

Pre-processed DW-MRI images were processed by fitting diffusion tensors (FSL's DTIFIT [54]) and by fitting a model of local fiber orientations including crossing fibers (FSL's BedpostX [55,56]). Up to three fiber orientations per voxel were allowed. Tractography was performed using FSL's probtrackx2. Registration warp-fields

between each subject's native space and standard space were created using FSL's FNIRT.

In five subjects of each species, we performed tractography of the following tracts (Figure 7B(1)): Cortico-spinal tract (CST), middle longitudinal fasciculus (MDLF), vertical occipital fasciculus (VOF), inferior fronto-occipital fasciculus (IFO), inferior longitudinal fasciculus (ILF), the third branch of the superior longitudinal fasciculus (SLF3), and the arcuate fasciculus (AF). The sample size was matched across species to keep the variability comparable. In the human, tractography was also performed for a larger sample of 20 subjects to validate the results (data not shown). Placement of seed, waypoint, and exclusion masks was based on previous studies, in order to reconstruct known pathways for these tracts in all three species (human and macaque: [16,57], protocols for AF: [7]; chimpanzee: Bryant, Li, & Mars, in prep.). Masks were drawn in standard space and warped to native subject diffusion MRI space for probabilistic tractography. The resulting tractograms were normalized by dividing each voxel's value by the total number of streamlines that successfully traced the required route ('waytotal'). To decrease computational load for further processing all tractograms were down-sampled (human: 2 mm, chimpanzee: 1.5 mm, macaque: 1 mm).

Surface Tract Maps

To assess which part of the cortical grey matter might be reached by the tracts, we derived the surface representation of each individual tractogram using a matrix multiplication approach described previously [16].

We calculated whole-hemisphere vertex-wise connectivity matrices, tracking from the 20k-vertices mid-thickness surface to all voxels in the brain. These matrices were computed for both hemispheres and each subject individually in the three species. In the macaque we used the five subject's average mid-thickness in standard space as input for the computation instead of individual surfaces.

To rebalance the weights in the tracts to be more homogenous, connectivity values were weighted by the distance between vertex and voxel. A distance matrix across all vertices of the mid-thickness surface and all brain voxels was computed using MATLAB's pdist2-function resulting in a matrix of the same size as the connectivity matrix. Each element in the connectivity matrix was then divided by the corresponding value in the vertex-to-voxel distance matrix. To decrease data storage load (approx. 10 GB per matrix) the weighted connectivity matrices of the five subjects were averaged for each hemisphere and species.

To visualize a tract's surface representation, we multiplied the averaged connectivity matrix with a tract's tractogram ('fdt_paths'). We refer to the tract surface representation here as 'tract map' (Figure 7B(2)). Tract maps were derived for each subject and hemisphere separately. The method introduced spurious effects on the medial wall and insula cortex, which are generally not well captured in the tract map. Given that both areas are not of interest in this study, they were masked out for further analysis. Individual surface maps were smoothed on the mid-thickness surface (human: 4 mm kernel (sigma for the gaussian kernel function), smoothing on individual

surface; chimpanzee: 3 mm kernel, smoothing on average surface; macaque: 2 mm kernel, smoothing on average surface), logNorm-transformed and averaged across subjects.

Predicted Tract Maps

Next, we tested if our myelin-based registration can be used to predict the tract maps across the three species. We resampled the average chimpanzee and macaque tract maps to human space using the macaque-to-human and the chimpanzee-to-human registration (Figure 7B(3)). Intensity values in actual and predicted tract maps ranged from 0 to 1. We displayed predicted tract maps onto a human average surface (Q1-Q6_R440), and for visual inspection we also assessed thresholded tract maps. Thresholds were chosen different for each tract, ranging from 0.6 to 0.85, so that the most characteristic termination is visible (Figure 7B(4)).

To visualize and quantify the prediction of macaque and chimpanzee tracts in human space, we derived weighted whole-hemisphere local correlation maps of the human map and the map predicted by macaque or chimpanzee (Figure 7B(4)). The local correlation map was computed as described above for the myelin maps using the same search kernel. The correlation map was modified to up-weight the brain areas where the tract is represented on the surface. A weighting mask was derived by multiplication of the intensities in the actual human tract map and the other species' predicted map. The values for the weighted correlation map are thus high in parts of the brain where both actual human and predicted tract show a termination, and where the spatial patterns of intensity values correlate.

In order to quantify how well a tract is predicted, we computed two measures based on the weighted correlation map: The median value of the weighted correlation map, here referred to as 'correlation value', and the Dice coefficient of similarity [59], which quantifies the amount of overlap of the tract maps. The Dice coefficient was computed for the binarized and thresholded weighted correlation map and the thresholded actual human tract map. We derived these metrics in an area defined by the thresholded actual human tract map (t = 0.2) to control for the general differences in spatial extend and distribution of the tract terminations. Both measures were computed for a range of thresholds to confirm that the pattern of values is robust.

Acknowledgements

N.E. is a Wellcome Trust Doctoral student in Neuroscience at the University of Oxford [203730/Z/16/Z]. The project was supported by the NIHR Oxford Health Biomedical Research Centre. The Wellcome Centre for Integrative Neuroimaging is supported by core funding from the Wellcome Trust (203139/Z/16/Z). The work of R.B.M. is supported by the Biotechnology and Biological Sciences Research Council (BBSRC) UK [BB/N019814/1] and the Netherlands Organization for Scientific Research NWO [452-13-015]. The work of E.C.R. was supported by the Academy of Medical Sciences/the British Heart Foundation/the Government Department of Business, Energy and Industrial Strategy/the Wellcome Trust Springboard Award

[SBF003\1116]. The work of K.L.B. is supported by a Marie Sklodowska-Curie Postdoctoral Research Fellowship from the European Commission [750026]. The work of S.J. is supported by the Medical Research Council UK [MR/L009013/1]. The work of M.J. is supported by the National Institute for Health Research (NIHR) Oxford Biomedical Research Centre (BRC). L.L.'s work is supported by the following grants: R01MH118534, P50MH100029, R01MH118285. Acquisition of the chimpanzee data was funded in part by the Yerkes National Primate Research Center Grant No. ORIP/OD P51OD011132; the Yerkes National Primate Center is supported by the National Institutes of Health, Office of Research Infrastructure Programs/OD [P51OD011132]; the National Chimpanzee Brain Resource is supported by NIH - National Institute of Neurological Disorders and Stroke. K.K.'s work is supported by the BBSRC UK [BB/H016902/1] and a Wellcome Trust Strategic Award [101092/Z/13/Z].

Author Contributions

Writing – Original draft: N.E., R.B.M.; Supervision and Project Administration: R.B.M.; Conceptualization: N.E., R.B.M.; Software: E.C.R.; Methodology: N.E., E.C.R., S.J., M.J., R.B.M.; Resources: N.E., K.L.B., L.L., K.K., R.B.M., K.E.W.; Writing – Review & Editing: N.E., E.C.R., K.L.B., S.J., M.J., K.K., K.E.W., R.B.M.; Funding Acquisition: N.E., R.B.M.

Declaration of Interests

The authors declare no competing interests.

Data Availability

All derived data supporting the findings of this study are available from the corresponding author upon request. Results scene files will be made available from the Wellcome Centre for Integrative Neuroimaging's GitLab at git.fmrib.ox.ac.uk/neichert/project_MSM.

Code Availability

Upon acceptance of the manuscript, code to run the between-species registration using MSM will be available from the Wellcome Centre for Integrative Neuroimaging's GitLab at git.fmrib.ox.ac.uk/neichert/project_MSM. FSL tools, including MSM, are available from fsl.fmrib.ox.ac.uk. Code for MSM using higher-order smoothness constrains is online available (https://www.doc.ic.ac.uk/~ecr05/MSM_HOCR_v2/). Connectome Workbench is available at www.humanconnectome.org/software/connectome-workbench.html.

Supplementary Material

Supplementary Methods

Myelin-based Surface Registration

We implemented a cross-species registration based on surface myelin maps using MSM. MSM is a cortical surface registration algorithm, which works by projecting sheet-like models of the cortical surface to spheres; then aligning these by driving deformation of an input (or moving) mesh until features on the surface (i.e. myelin map intensities) increase in similarity with those represented on a fixed, or reference, mesh. We used a version of MSM that uses higher-order smoothness constraints and strain-based regularization for the regularization mode. MSM can work with multidimensional feature maps and use cross correlation across features to drive a registration. Multiple registration steps can be combined by using the output of a previous registration as initialization.

The main inputs of MSM were the average species myelin maps (Figure S1(1)). All surface and metric files were resampled to a regular 20k-vertices mesh (radius of the sphere: 10 cm). For all species, the same sphere was used for re-sampling, so that the vertices had correspondence across species (Figure S1(2)).

Given the substantial distortions that are required to match myelin landmarks across species, we initialized the myelin registration using a region-of-interest-(ROI)-driven registration. Three binary ROIs were manually drawn in Connectome Workbench's wb_view onto each species' myelin map (Figure S1(3)). The value inside the ROI was 1 and outside 0. Two ROIs captured the highly myelinated precentral motor cortex (MC) and MT+ complex and a third ROI covered the medial wall (MW). The first initialization step aligned a single ROI for MT+ complex between species to facilitate alignment of the remaining two ROIs (Figure S1(5)). Next, the three ROIs were combined in a multidimensional file, i.e. in a metric file that contained three data-arrays, or columns (Figure S1(6)). MSM alignment of these sets of ROIs was initialized by the MT+ ROI registration (Figure S1(9)). Initialization was performed using the '--trans=X.sphere.reg.surf.gii'-setting in the MSM-command. In the following step, the whole-hemisphere myelin maps were aligned by using the three-ROI registration step as initialization (Figure S1(10)).

To derive a macaque-to-human registration, we resampled the macaque myelin map to chimpanzee space using the MSM-derived macaque-to-chimpanzee registration. Then we registered the resampled macaque map to the human map while using the chimpanzee-to-human registration as initialization. This approach allowed refinement of the macaque-to-human mapping rather than just applying the chimpanzee-to-human registration to the resampled map. The surface registration was derived for both hemispheres separately with mirrored versions of the ROIs. For registration steps involving ROIs, the registration sphere derived from the left hemisphere was flipped to the right hemisphere. For the steps using myelin maps, we derived the registration separately for the right hemisphere. Configuration parameters for all MSM-steps were

determined empirically and were kept constant for the two hemispheres (all parameters are provided in Table S2).

Supplementary Figure

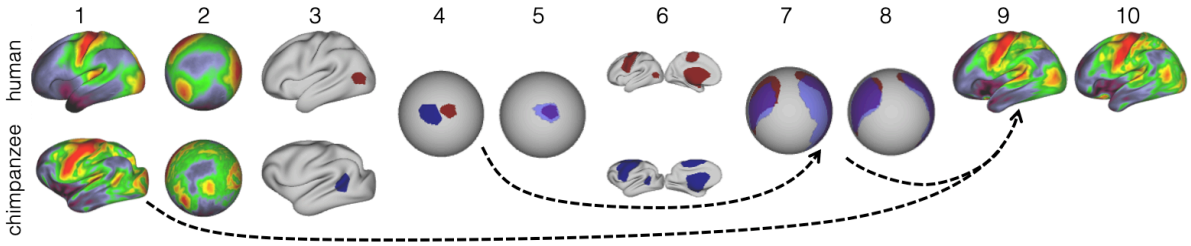

Figure S1. Related to Figure 7. MSM registration between chimpanzee and human myelin maps. (1) average species myelin maps. (2) myelin maps displayed on common sphere. (3) ROI for MT+ complex drawn on native surface. (4) MT+ ROI displayed on common sphere. (5) chimpanzee MT+ ROI (blue) registered to human (red) using MSM. (6) Set of three ROIs (MC, MT+, MW). (7) Effect of MT+ ROI-derived initialization on the set of ROIs (only MW and MC visible). (8) Registration of chimpanzee set of ROIs to human ROIs using MSM. (9) Effect of ROI-derived registration on whole hemisphere chimpanzee myelin map. (10) Registration of whole brain myelin maps initialized by set of ROIs using MSM. The dashed lines indicate a registration warp between two steps that is applied later to create a novel map.

Supplementary Tables

sulcal depth	myelin map
--simval=1,2,2,2 --sigma_in=4,4,2,1 --sigma_ref=2,2,1,1 --lambda=0,0.1,0.2,0.3 --it=50,3,3,3 --opt=AFFINE,DISCRETE,DISCRETE,DISCRETE --CPgrid=0,2,3,4 --SGgrid=0,4,5,6 --datagrid=4,4,5,6 --IN levels=4	--simval=2,2,2 --sigma_in=10,5,3 --sigma_ref=10,5,3 --lambda=0.1,0.1,0.3 --it=10,10,10 --opt=DISCRETE,DISCRETE,DISCRETE --CPgrid=2,3,4 --SGgrid=4,5,6 --datagrid=4,5,6 levels=3 (--trans: sulcal depth registration)

Table S1. Related to Methods. MSM configuration parameters for the registration of individual subject myelin maps prior to averaging to create a species myelin map. The parameters were kept constant for the three species and for both hemispheres.

macaque mesh as input	chimpanzee mesh as input
step: 4→5 macaque-to-chimpanzee: MT+ ROI --sigma_in=25 --lambda=0.1 --it=10 --opt=DISCRETE --CPgrid=1 --SGgrid=3 --regoption=3 --regexp=2 --dopt=HOCR --VN	step: 4→5 chimpanzee-to-human: MT+ ROI --sigma_in=20,15,5 --lambda=0.05,0.1,0.1 --it=10,10,10 --opt=DISCRETE,DISCRETE,DISCRETE --CPgrid=2,3,4 --SGgrid=4,5,6 --regoption=3 --regexp=2 --dopt=HOCR --VN

--triclique --k_exponent=2 --bulkmod=1 --shearmod=0.2 level=1	--triclique --k_exponent=2 --bulkmod=1 --shearmod=0.2 level=3
step: 7→8 macaque-to-chimpanzee: three ROIs --sigma_in=25,15,5 --lambda=0.01,0.01,0.1 --it=10,10,10 --opt=DISCRETE,DISCRETE,DISCRETE --CPgrid=1,2,3 --SGgrid=3,4,5 --regoption=3 --regexp=2 --dopt=HOCR --VN --triclique --k_exponent=2 --bulkmod=1 --shearmod=0.1 level=3 (--trans: single ROI registration)	step: 7→8 chimpanzee-to-human: three ROIs --sigma_in=25 --lambda=0.001 --it=10 --opt=DISCRETE --CPgrid=2 --SGgrid=4 --regoption=3 --regexp=2 --dopt=HOCR --VN --triclique --k_exponent=2 --bulkmod=1 --shearmod=0.2 level=1 (--trans: single ROI registration)
step: 9→10 macaque-to-chimpanzee: myelin map --sigma_in=10,5,3 --lambda=0.1,0.1,0.1 --it=10,10,20 --opt=DISCRETE,DISCRETE,DISCRETE --CPgrid=2,3,4 --SGgrid=4,5,6 --IN --excl --regoption=3 --regexp=2 --dopt=HOCR --triclique --k_exponent=2 --bulkmod=1 --shearmod=0.2 level=3 (--trans: three ROI registration)	step: 9→10 chimpanzee-to-human: myelin map --sigma_in=25,10,5 --lambda=0.2,0.5,0.5 --it=10,10,10 --opt=DISCRETE,DISCRETE,DISCRETE --CPgrid=2,3,4 --SGgrid=4,5,6 --regoption=3 --regexp=2 --dopt=HOCR --triclique --k_exponent=2 --bulkmod=1.6 --shearmod=0.1 level=3 (--trans: three ROI registration)
step: 9→10 macaque-to-human (input: macaque myelin map transformed by applying the macaque-to-chimpanzee registration) --sigma_in=25,10,5 --sigma_ref=25,10,5 --lambda=0.1,0.1,0.1 --it=10,10,3 --opt=DISCRETE,DISCRETE,DISCRETE --CPgrid=2,3,4 --SGgrid=4,5,6 --datagrid=4,5,6 --IN --regoption=3	

--regexp=2 --dopt=HOCR --triclique --k_exponent=2 --bulkmod=1.6 --shearmod=0.1 level=3 (--trans: chimpanzee-to-human myelin map registration)	

Table S2. Related to Methods 'Myelin-based Surface Registration'. MSM configuration parameters. Settings for the MSM command for registrations using the macaque data as input (left panel) and chimpanzee data as input (right panel). The described 'step' refers to the numbering in Figure S1. Parameters were identical for the left and right hemisphere.

References

1. Krubitzer, L. In search of a unifying theory of complex brain evolution. *Annals of the New York Academy of Sciences* **1156**, 44–67 (2009).
2. Krubitzer, L. & Kaas, J. The evolution of the neocortex in mammals: How is phenotypic diversity generated? *Current Opinion in Neurobiology* **15**, 444–453 (2005).
3. Mars, R. B., Passingham, R. E., Neubert, F. X., Verhagen, L. & Sallet, J. Evolutionary specializations of the human association cortex. in *Evolution of Nervous Systems* (ed. Kaas, H. J.) 1–37 (Elsevier, 2017). doi:10.1016/B978-0-12-804042-3.00118-4
4. Mars, R. B., Eichert, N., Jbabdi, S., Verhagen, L. & Rushworth, M. F. S. Connectivity and the search for specializations in the language-capable brain. *Current Opinion in Behavioral Sciences* **21**, 19–26 (2018).
5. Huk, A. C., Dougherty, R. F. & Heeger, D. J. Retinotopy and functional subdivision of human areas MT and MST. *The Journal of neuroscience : the official journal of the Society for Neuroscience* **22**, 7195–205 (2002).
6. Striedter, G. F. *et al.* NSF workshop report: Discovering general principles of nervous system organization by comparing brain maps across species. *Journal of Comparative Neurology* **522**, 1445–1453 (2014).
7. Eichert, N. *et al.* What is special about the human arcuate fasciculus? Lateralization, projections, and expansion. *Cortex* 1–9 (2018). doi:10.1016/j.cortex.2018.05.005
8. Robinson, E. C. *et al.* MSM: A new flexible framework for multimodal surface matching. *NeuroImage* **100**, 414–426 (2014).
9. Robinson, E. C. *et al.* Multimodal surface matching: Fast and generalisable cortical registration using discrete optimisation. in *Lecture Notes in Computer Science (including subseries Lecture Notes in Artificial Intelligence and Lecture Notes in Bioinformatics)* **7917 LNCS**, 475–486 (2013).
10. Robinson, E. C. *et al.* Multimodal surface matching with higher-order smoothness constraints. *NeuroImage* **167**, 453–465 (2018).
11. Thiebaut de Schotten, M., Croxson, P. L. & Mars, R. B. Large-scale comparative neuroimaging: Where are we and what do we need? *Cortex* (2019). doi:10.1016/j.cortex.2018.11.028
12. Glasser, M. F. & Van Essen, D. C. Mapping Human Cortical Areas In Vivo Based on Myelin Content as Revealed by T1- and T2-Weighted MRI. *Journal of Neuroscience* **31**, 11597–11616 (2011).
13. Glasser, M. F., Goyal, M. S., Preuss, T. M., Raichle, M. E. & Van Essen, D. C. Trends and properties of human cerebral cortex: Correlations with cortical myelin content. *NeuroImage* **93**, 165–175 (2014).
14. Large, I. *et al.* Individual Differences in the Alignment of Structural and Functional Markers of the V5/MT Complex in Primates. *Cerebral Cortex* **26**, 3928–3944 (2016).
15. Hecht, E. E., Gutman, D. A., Bradley, B. A., Preuss, T. M. & Stout, D. Virtual dissection and comparative connectivity of the superior longitudinal fasciculus in chimpanzees and humans. *NeuroImage* **108**, 124–137 (2015).
16. Mars, R. B. *et al.* Whole brain comparative anatomy using connectivity

blueprints. *eLife* **7**, (2018).
17. Mars, R. B. *et al.* Connectivity-based subdivisions of the human right 'temporoparietal junction area': Evidence for different areas participating in different cortical networks. *Cerebral Cortex* **22**, 1894–1903 (2012).
18. Ruschel, M. *et al.* Connectivity architecture and subdivision of the human inferior parietal cortex revealed by diffusion MRI. *Cerebral Cortex* **24**, 2436–2448 (2014).
19. Mars, R. B., Sallet, J., Neubert, F. X. & Rushworth, M. F. S. Connectivity profiles reveal the relationship between brain areas for social cognition in human and monkey temporoparietal cortex. *Proceedings of the National Academy of Sciences* **110**, 10806–10811 (2013).
20. Van Essen, D. C. & Dierker, D. L. Surface-Based and Probabilistic Atlases of Primate Cerebral Cortex. *Neuron* **56**, 209–225 (2007).
21. Rilling, J. K. *et al.* The evolution of the arcuate fasciculus revealed with comparative DTI. *Nature Neuroscience* **11**, 426–428 (2008).
22. Mars, R. B. *et al.* The extreme capsule fiber complex in humans and macaque monkeys: a comparative diffusion MRI tractography study. *Brain Structure and Function* **221**, 4059–4071 (2016).
23. Hecht, E. E. *et al.* Process versus product in social learning: comparative diffusion tensor imaging of neural systems for action execution-observation matching in macaques, chimpanzees, and humans. *Cerebral cortex (New York, N.Y. : 1991)* **23**, 1014–24 (2013).
24. Bryant, K. & Mars, R. B. Organization of extrastriate and temporal cortex in chimpanzees compared to humans and macaques (in press). *Cortex* (2019).
25. Makris, N. *et al.* Human middle longitudinal fascicle: Segregation and behavioral-clinical implications of two distinct fiber connections linking temporal pole and superior temporal gyrus with the angular gyrus or superior parietal lobule using multi-tensor tractography. *Brain Imaging and Behavior* **7**, 335–352 (2013).
26. Mars, R. B., Passingham, R. E. & Jbabdi, S. Connectivity Fingerprints: From Areal Descriptions to Abstract Spaces. *Trends in Cognitive Sciences* **22**, 1026–1037 (2018).
27. Hagoort, P. MUC (memory, unification, control) and beyond. *Frontiers in Psychology* **4**, 1–13 (2013).
28. Roelofs, A. A dorsal-pathway account of aphasic language production: The WEAVER++/ARC model. *Cortex* **59**, 33–48 (2014).
29. Catani, M. & Bambini, V. A model for Social Communication And Language Evolution and Development (SCALED). *Current Opinion in Neurobiology* **28**, 165–171 (2014).
30. Makris, N. & Pandya, D. N. The extreme capsule in humans and rethinking of the language circuitry. *Brain Structure and Function* **213**, 343–358 (2009).
31. Saur, D. *et al.* Ventral and dorsal pathways for language. *Proceedings of the National Academy of Sciences of the United States of America* **105**, 18035–40 (2008).
32. Glasser, M. F. *et al.* A multi-modal parcellation of human cerebral cortex. *Nature* **536**, 171–178 (2016).
33. Abdollahi, R. O. *et al.* Correspondences between retinotopic areas and myelin maps in human visual cortex. *NeuroImage* **99**, 509–524 (2014).
34. Garcia, K. E. *et al.* Dynamic patterns of cortical expansion during folding of the preterm human brain. *Proceedings of the National Academy of Sciences* **115**,

3156–3161 (2018).
35. Zhang, H., Schneider, T., Wheeler-Kingshott, C. A. & Alexander, D. C. NODDI: Practical in vivo neurite orientation dispersion and density imaging of the human brain. *NeuroImage* **61**, 1000–1016 (2012).
36. Vincent, J. L. *et al.* Intrinsic functional architecture in the anaesthetized monkey brain. *Nature* **447**, 83–86 (2007).
37. Heuer, K. *et al.* Evolution of neocortical folding: A phylogenetic comparative analysis of MRI from 33 primate species. *bioRxiv* 379750 (2018). doi:10.1101/379750
38. Milham, M. P. *et al.* An Open Resource for Non-human Primate Imaging. *Neuron* **100**, 61-74.e2 (2018).
39. Miller, K. L. *et al.* Multimodal population brain imaging in the UK Biobank prospective epidemiological study. *Nature Neuroscience* **19**, 1523–1536 (2016).
40. Stejskal, E. O. & Tanner, J. E. Spin diffusion measurements: spin echoes in the presence of a time-dependant field gradient. *The Journal of chemical physics* **42**, 288–292 (1965).
41. Glasser, M. F. *et al.* The minimal preprocessing pipelines for the Human Connectome Project. *NeuroImage* **80**, 105–124 (2013).
42. Fischl, B. FreeSurfer. *NeuroImage* **62**, 774–781 (2012).
43. Jenkinson, M., Beckmann, C. F., Behrens, T. E. J., Woolrich, M. W. & Smith, S. M. FSL. *NeuroImage* **62**, 782–790 (2012).
44. Donahue, C. J., Glasser, M. F., Preuss, T. M., Rilling, J. K. & Van Essen, D. C. Quantitative assessment of prefrontal cortex in humans relative to nonhuman primates. *Proceedings of the National Academy of Sciences* **115**, E5183–E5192 (2018).
45. Li, L. *et al.* Mapping putative hubs in human, chimpanzee and rhesus macaque connectomes via diffusion tractography. *NeuroImage* **80**, 462–474 (2013).
46. Mars, R. B. *et al.* Concurrent analysis of white matter bundles and grey matter networks in the chimpanzee. *Brain Structure and Function* **0**, 0 (2018).
47. de Crespigny, A. J. *et al.* Acute studies of a new primate model of reversible middle cerebral artery occlusion. *Journal of stroke and cerebrovascular diseases : the official journal of National Stroke Association* **14**, 80–7 (2005).
48. Jbabdi, S., Lehman, J. F., Haber, S. N. & Behrens, T. E. Human and Monkey Ventral Prefrontal Fibers Use the Same Organizational Principles to Reach Their Targets: Tracing versus Tractography. *The Journal of neuroscience : the official journal of the Society for Neuroscience* **33**, 3190–3201 (2013).
49. Donahue, C. J. *et al.* Using Diffusion Tractography to Predict Cortical Connection Strength and Distance: A Quantitative Comparison with Tracers in the Monkey. *The Journal of Neuroscience* **36**, 6758–6770 (2016).
50. Ishikawa, H. Higher-order clique reduction without auxiliary variables. *Proceedings of the IEEE Computer Society Conference on Computer Vision and Pattern Recognition* 1362–1369 (2014). doi:10.1109/CVPR.2014.177
51. Smith, S. M. *et al.* Advances in functional and structural MR image analysis and implementation as FSL. in *NeuroImage* **23**, S208–S219 (2004).
52. Andersson, J. L. R., Skare, S. & Ashburner, J. How to correct susceptibility distortions in spin-echo echo-planar images: Application to diffusion tensor imaging. *NeuroImage* **20**, 870–888 (2003).
53. Andersson, J. L. R. & Sotiropoulos, S. N. An integrated approach to correction for off-resonance effects and subject movement in diffusion MR imaging.

NeuroImage **125**, 1063–1078 (2016).
54. Behrens, T. E. J. *et al.* Characterization and Propagation of Uncertainty in Diffusion-Weighted MR Imaging. *Magnetic Resonance in Medicine* **50**, 1077–1088 (2003).
55. Behrens, T. E. J., Johansen-Berg, H., Jbabdi, S., Rushworth, M. F. S. & Woolrich, M. W. Probabilistic diffusion tractography with multiple fibre orientations: What can we gain? *NeuroImage* **34**, 144–155 (2007).
56. Jbabdi, S., Sotiropoulos, S. N., Savio, A. M., Graña, M. & Behrens, T. E. J. Model-based analysis of multishell diffusion MR data for tractography: How to get over fitting problems. *Magnetic Resonance in Medicine* **68**, 1846–1855 (2012).
57. De Groot, M. *et al.* Improving alignment in Tract-based spatial statistics: Evaluation and optimization of image registration. *NeuroImage* **76**, 400–411 (2013).
58. Bryant, K. L., Li, L. & Mars, R. B. A white matter atlas of the chimpanzee brain and quantitative comparison with human and macaque (in prep).
59. Dice, L. R. Measures of the Amount of Ecologic Association Between Species. *Ecology* **26**, 297–302 (1945).